Journal of Ceramic Processing Research. Vol. 8, No. 3, pp. 224-228 (2007)

J O U R N A L O F
Ceramic Processing Research

Computer modeling of single-chamber SOFCs with hydrocarbon fuel

Jeong-Hwa Cha[1,2], Yong-Chae Chung[1,*], Hye-Ryung Kim[2], Ji-Won Son[2], Joosun Kim[2], Jong-Ho Lee[2] and Hae-Weon Lee[2]

[1]*Department of Materials Science and Engineering, Hanyang University, Seoul 133-791, Korea*
[2]*Nano-Materials Research Center, Korea Institute of Science and Technology, Seoul 136-791, Korea*

The modeling of a single-chamber SOFC has been performed under various fuel/air mixing ratios. Specifically, the energy and mass balance of a single-chamber solid oxide fuel cell (SC-SOFC) were investigated. Electrodes with selective catalytic activity were adapted and dry methane and oxygen mixture diluted by N_2 was prepared as a fuel. The temperature and gas concentration for the reforming reactions, the water-gas shift reaction, and electrochemical reactions were calculated by a numerical model. Fluid dynamics, heat conduction convection, and mass diffusion convection were considered in the frame of a Finite Element Method (FEM). Through the numerical approach of a SOFC with hydrocarbon fuel, the reactant and product gas distribution, the temperature distribution and cell performance with catalytically active electrodes were successfully predicted. Using the calculated the concentration distribution and the temperature distribution, ohmic loss, activation loss and concentration loss were obtained.

Key words: micro single-chamber solid oxide fuel cell, hydrocarbon fuel, numerical analysis.

Introduction

A solid oxide fuel cell (SOFC) is a highly efficient energy system that directly converts chemical energy to electrical energy. A SOFC is operated at high temperature above 800 °C and is made with catalytically active electrodes such as nickel. Thus a SOFC needs no external reformer, due to the internal catalytic reforming process. The widely-employed steam reforming (SR) method, which is an endothermic reaction, requires an external heat source. On the other hand, dry reforming using only dry oxygen for the oxidant, which is an exothermic reaction, has advantages in operating a SOFC [1, 2]. There are two approaches to internal reforming with the catalytic reforming of hydrocarbon. One is integrated internal reforming (IIR) that produces hydrogen by a separated reformer adjacent to the anode, and the other is direct internal reforming (DIR) that utilizes the fuel directly injected into the cell [3].

Recently, the idea of a single-chamber SOFC has been of great interest due to the simplicity of the cell configuration which requires no sealing between the anode and cathode compartments. This promising concept had not been realized until Hibino et al. mainly because of the lack of basic understanding of operation principle of single-chamber SOFC [4].

In this study, considering DIR in a micro-scale single cell, the gas distribution, the temperature distribution and the polarization characteristics were investigated through a numerical approach with a variation of the mixing ratio in the fuel/air mixture.

Calculation Model

A single-chamber model with electrodes placed on one side of electrolyte was employed for simulation (Fig. 1). The porous catalytic electrodes were prepared for the efficient methane reforming and electrochemical reactions. A fully dense and nonporous electrolyte was assumed for no gas species to penetrate into the electrolyte. The dimensions of the model for this study are indicated in Fig. 1. In the calculation, NiO-YSZ cermet with Pd and LSM-YSZ were adapted as electrodes and YSZ was employed as the electrolyte. Injected fuel gas was composed of a methane-air mixture, and nitrogen was used as the carrier gas. The cell operating temper-

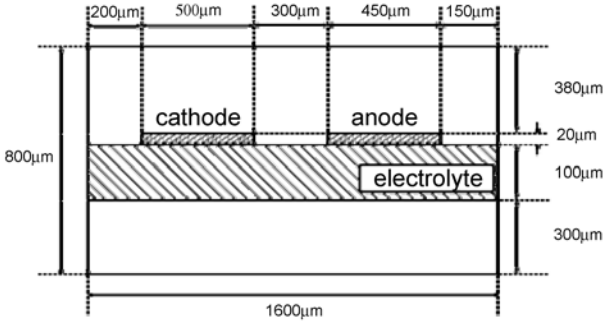

Fig. 1. The structure of the SOFC model employed in this study.

*Corresponding author:
Tel : +82-2-2220-0507
Fax: +82-2-2281-5308
E-mail: yongchae@hanyang.ac.kr

Table 1. Reactions involved in a single-chamber SOFC

Partial oxidation	(i) $CH_4+0.5O_2 \xrightarrow{k_{POX}} CO+2H_2$
Steam reforming	(ii) $CH_4+H_2O \xrightarrow{k_{SR}} CO+3H_2$
Water-Gas shift reaction	(iii) $CO+H_2O \xleftrightarrow{K_{shift}} CO_2+H_2$
Electrochemical reaction	(iv) $H_2+1/2O_2 \rightarrow H_2O$
(Hydrogen oxidation at anode)	$H_2+O^{2-} \rightarrow H_2O+2e^-$
(Oxygen reduction at cathode)	$1/2O_2+2e^- \rightarrow O^{2-}$

ature was varied from 1073 K to 1173 K by the heat produced from the electrodes reactions.

Reaction kinetics

It was assumed that 3 reactions occurred at the anode, partial oxidation of the fuel steam reforming the fuel, a water-gas shift reaction, and an electrochemical reaction, and one reaction at the cathode, an oxygen reduction reaction [3, 5, 6]. The gas-phase reactions in the gas channel were not considered in this study. Detailed corresponding electrode reactions and reaction kinetics are represented in Tables 1 and 2.

The reaction-rate equation was obtained from the literature [7-9]. Interestingly, only a few researches have been performed concerning the fuel reforming utilizing partial oxidation within a Ni composite anode. In this study, a Pd catalyst was added to improve the catalytic activity of anode. In addition, the partial oxidation using the Pd catalyst was mainly considered due to the higher catalytic activity for fuel reforming in comparison with a Ni catalyst.

Mass balance

The concentration flux of the given components within electrodes and the gas channel was determined by the Maxwell-Stefan equation (Eqn. 1). The gas species were assumed to be ideal and an incompressible fluid. The gas was injected with various R_{mix} ratios. The R_{mix} is the ratio of oxygen and methane (oxygen/methane). The injected gas mixture was composed of methane, air, and nitrogen. The specific ratios of each gas are summarized in Table 3. In the modeling, a total amount of 280 sccm was injected into the gas channel.

$$\frac{\partial \rho w_i}{\partial t}+\nabla\cdot(\mathbf{j}_i+\rho w_i\mathbf{u})=R_i \tag{1}$$

Momentum balance

The velocity distribution used in the mass balance was calculated by the Navier-Stoke equation (Eqn. 2) in the gas channel and the Darcy's law at the porous electrodes (Eqn. 3).

$$\rho(\mathbf{u}\cdot\nabla\mathbf{u})-\nabla\eta(\nabla\mathbf{u}+(\nabla\mathbf{u})^T+\nabla P)=0 \tag{2}$$

$$\nabla\cdot\left(-\frac{\kappa}{\eta}\nabla P\right)=0 \tag{3}$$

Energy balance

The heat flux in the gas channel and electrodes was determined by the heat transfer equation. Only the heat conduction (Eqn. 4) was considered at the cell components because the heat conductivity of the gas is generally less than that of the cell components. In the gas channel, heat convection and conduction (Eqn. 5) were applied.

$$\rho C_p\frac{\partial T}{\partial t}+\nabla\cdot(-\lambda\nabla T)=Q,\ Q=\sum_{i=1}^{4}h_i r_i \tag{4}$$

$$\rho C_p\frac{\partial T}{\partial t}+\nabla\cdot(-\lambda\nabla T+\rho C_p T\mathbf{u})=Q \tag{5}$$

Open circuit voltage (OCV)

The OCV was determined by the Nernst equation with the partial pressures of gas components (Eqn. 6). The fuel reforming through partial oxidation was only considered in order to calculate the OCV [10].

$$OCV=-\frac{\Delta G}{nF}=-\frac{\Delta G^0}{nF}+\frac{RT}{nF}\ln\frac{p_{H_2}p_{O_2}^{1/2}}{p_{H_2O}} \tag{6}$$

Overpotentials

Each loss was calculated from the numerical modeling

Table 3. Initial mass fraction employed in this study

	Mass fraction				
	Case1	Case2	Case3	Case4	Case5
CH_4	0.19	0.16	0.14	0.11	0.09
O_2	0.06	0.06	0.07	0.08	0.09
N_2	0.75	0.78	0.79	0.81	0.82
R_{mix}	3.167	2.667	2.00	1.375	1.00

Table 2. Reaction kinetics at the electrodes

Reaction rate	Rate & equilibrium constant
$R_{POx}=R_{(i)}=k_{(i)}[CH_4][O_2]^{0.5}$	$k_{(i)}=2.747\times10^6\exp\left(-\frac{40232}{RT}\right)$
$R_{SR}=R_{(ii)}=k_{(ii)}[CH_4(vol\%)]$	$k_{(ii)}=4.259\times10^{10}\exp\left(-\frac{162123.2}{RT}\right)$
$R_{shift}=R_{(iii)}=k_{(iii)}[CO]1-\frac{[CO_2][H_2]/[CO][H_2O]}{K_{eq(iii)}}$	$k_{eq(iii)}=1.767\times10^{-2}\exp\left(\frac{4400}{RT}\right)$
$R_{EC}=R_{(iv)}=\frac{i}{nF}$	

using commercial Finite Element Method (FEM) tools. The ohmic overpotential is due to the resistance of the cell components. The ohmic overpotential could be calculated from the current continuity equation, (Eqn. 7) [11]. Here, the ionic conductivity of the electrolyte and the electronic conductivity of the electrodes depend strongly on temperature and dimensions.

$$-\nabla\cdot(\sigma\nabla V_{ohm})=0 \tag{7}$$

The activation overpotential is caused by overcoming the energy barrier during the electrochemical reaction. The relation between the energy barrier and the activation overpotential is represented in the Butler-Volmer equation (Eqn. 8) [11].

$$i_e=i_{0,a}\exp\left(\alpha_a\frac{FV_{act}}{RT}\right)-i_{0,c}\exp\left(-\alpha_c\frac{FV_{act}}{RT}\right) \tag{8}$$

The concentration difference due to gas diffusion between gas channel and electrodes leads to the concentration overpotential. From the numerical data with the balance equations, the concentration overpotential was calculated through Eqn. 9 [12].

$$V_{con,a}=\frac{RT}{nF}\ln\left(\frac{p_{H_2O,TPB}p_{H_2,channel}}{p_{H_2O,channel}p_{H_2,TPB}}\right) \tag{9}$$

$$V_{con,c}=\frac{RT}{2nF}\ln\left(\frac{p_{O_2,channel}}{p_{O_2,TPB}}\right)$$

Results and Discussion

Concentration distribution

The calculated mole fraction of case3 corresponding to the operating temperature in the position of the cell at 2000 A/m^2 was shown in Fig. 2. The mole fraction of the gas component was dramatically changed at the anode because most of the reactions occurred at the anode, on the other hand, at the cathode, only the consumption of oxygen occurred. The heat from the partial oxidation and the heat convection led to the increment of the cell temperature, thus the conversion of hydrogen from methane and the ionization of oxygen increased along the cell length. And the hydrocarbon fuel was nearly all changed to hydrogen to use the electrochemical reactions by the reforming reaction, so the distribution of mole fraction was slightly changed

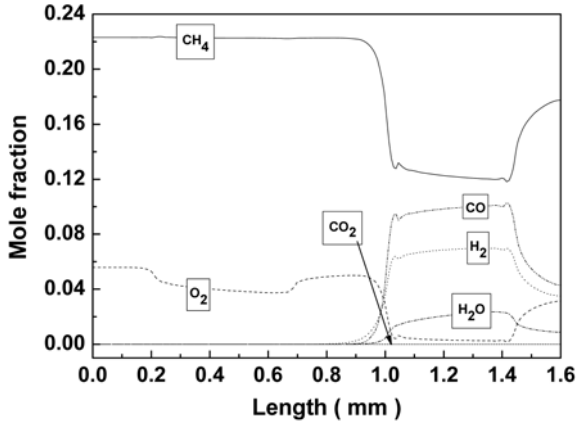

Fig. 2. The distribution of mole fraction in the direction of the cell during operation cell for case3 in Table 3 at 1073 K, 1123 K, or 1173 K, which turned out to be very similar and coincide with each other. (The x-axis is represented as same as the horizontal dimension of Fig. 1.)

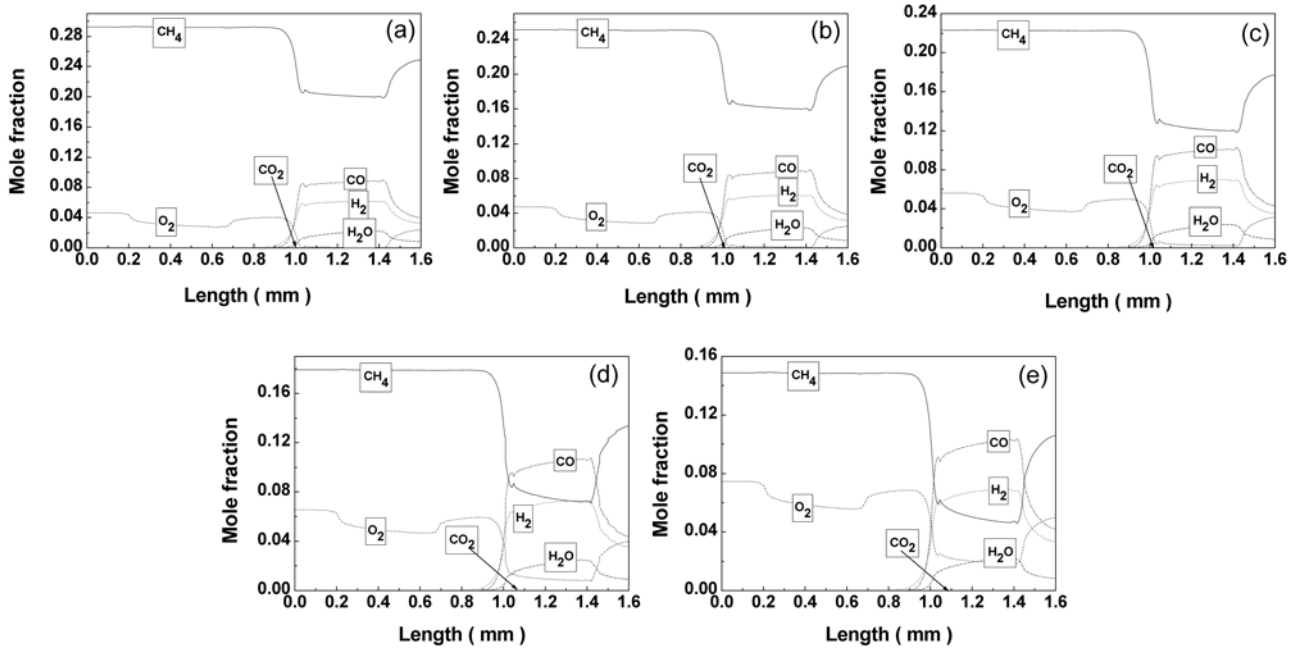

Fig. 3. The distribution of mole fraction in the direction of the cell during operation cell at 1123 K and 2000 A/m^2 for (a) case1 (b) case2 (c) case3 (d) case4, and (e) case5 in Table 3. (The x-axis is represented as same as the horizontal dimension of Fig. 1.)

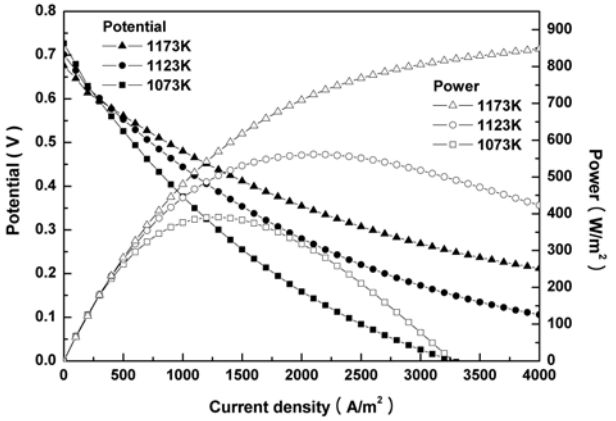

Fig. 4. The polarization curve considering both the reforming reaction and the electrochemical reaction for case3 in Table 3. (Other cases in Table 3 showed a very similar trend.)

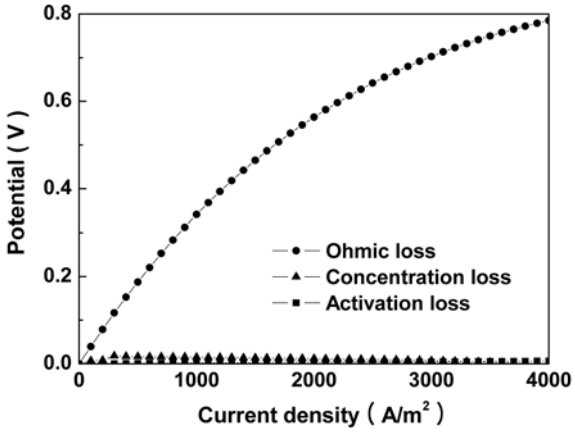

Fig. 5. Each loss as a function of current density at 1073 K for case3 in Table 3.

with the variation of the operating temperature.

The distribution of gases produced was affected by the ratio of the mixed fuel gas (R_{mix}). Because the current density used in this study was lower than the nominal experimental value, a smaller amount of steam was produced in the steam reforming process, and the partial oxidation turned out to be dominant process in the reforming reaction. As shown in Fig. 3, the hydrogen production increased according to a decreasing R_{mix} (a $\rightarrow$ e). Also it was found that the mole fraction of hydrogen and carbon monoxide (the product gas from the reforming reactions) reached a maximum at R_{mix}=2 that was the stoichiometric ratio for the corresponding steam reforming.

Cell performance

The polarization curve corresponding to the variation of current density for the case3 in Table 3 is presented Fig. 4. In the temperature range below 1073 K, the OCV characteristic cannot be found out due to the high partial pressure of oxygen, in other words, the temperature was not sufficiently high to activate the partial oxidation process of methane at the Ni cermet electrode. However, the operating potential rapidly decreased at 1073 K but as the temperature increased, and the potential and the power density were increased more than twice, especially above 1173 K. The operating voltage and the power density were increased with R_{mix} close to 1, which was caused by decreasing the ohmic overpotential due to the temperature increment according to the decrement of R_{mix}. Interestingly, other cases of Table 3 (case1, case2, case4, and case5) showed a very similar trend, hence they were not represented here separately.

Figure 5 shows that the ohmic overpotential was the major loss for the cell performance on the polarization curve for the SOFC configuration employed. The activation overpotential was much smaller than the ohmic overpotential and the potential curve linearly declines according to the increment of the current density due to the small activation overpotential. The concentration overpotential was minimal because the mixed gas was injected into one chamber and the gas mixture reacted with the whole volume of electrodes.

Conclusions

The distribution of gases during the operation of a cell was calculated by numerical simulation based on macro modeling of multi-physical phenomena. The hydrogen production and, consequently, the cell performance increased with R_{mix} and reached a maximum value of R_{mix} (R_{mix}=2). A high temperature was also found to be beneficial for the cell performance. However, only a little change of mole fraction distribution could be found because the operating temperature range adapted in this study was sufficiently high to reform the mixed fuel gas. In general, a higher R_{mix} is preferred in an experimental environment for effective gas mixing of reactant and product gases in a single-chamber SOFC. However, it turned out that the maximum hydrogen production and cell performance was presented near to R_{mix}=2. It was expected that the computational scheme developed in this study, may serve as a guideline for manufacturing micro scale single-chamber SOFC systems and optimizing the proper operating ranges of fuel/air mixtures.

Acknowledgement

This work was supported by the research fund of Hanyang University (HY-2005-M).

Nomenclature

η : dynamic viscosity [Pa·s]
κ : permeability [m^2]
λ : thermal conductivity [W/m·K]
ρ : density [kg/m^3]
σ : conductivity [S/m]

C_p : heat capacity [J/K]
F : Faraday constant [C/mol]
a_i : activity of species i
G_i : Gibbs free energy of species i [J/mol]
h_i : heat transfer coefficient [W/m^2·K]
i_e : current density [A/m^2]
i_0 : exchange current density [A/m^2]
n : the number of electrons transferred in the electrochemical reaction
P : pressure [Pa]
p : partial pressure of species i
R : gas constant [J/mol·K]
T : temperature [K]
u : velocity vector [m/s]
V : voltage [V]
w_i : mass fraction of species i

Subscripts

a : properties at the anode
act : activation
c : properties at the cathode
con : concentration
eff : effective parameter in the porous media
ohm : ohmic

References

1. J.R. Rostrup-Nielsen and L.J. Christiansen, Appl. Catal. A: Gen. 126[2] (1995) 381-390.
2. S.H. Clarke, A.L. Dicks, K. Pointon, T.A. Smith, and A. Swann, Catal. Today 38[4] (1997) 411-423.
3. S.C. Singhal and K. Kendall, in "High-temperature Solid Oxide Fuel Cells: Fundamentals, Design and Applications" (Elsevier Science, 2004).
4. T. Hibino, A. Hashimoto, T. Inoue, J.-I. Tokuno, S.-I. Yoshida, and M. Sano, Science 288[5473] (2000) 2031-2033.
5. A.L. Dicks, J. Power Sources 71[1-2] (1998) 111-122.
6. W. Lehnert, J. Meusinger and F. Thom, J. Power Sources 87[1-2] (2000) 57-63.
7. V.D. Belyaev, T.I. Politova, O.A. Mar'ina, and V.A. Sobyanin, Appl. Catal. A: Gen. 133[1] (1995) 47-57.
8. K. Hou and R. Hughes, Chem. Eng. J. 82[1-3] (2001) 311-328.
9. R.E. Hayes, S.T. Kolaczkowski, P.K.C. Li, and S. Awdry, Chem. Eng. Sci. 56[16] (2001) 4815-4835.
10. J. Larminie and A. Dicks, in "Fuel Cell System Explained" (2nd ed., John Wiley and Sons Ltd, England, 2003).
11. H. Zhu and R.J. Kee, J. Power Sources 117[1-2] (2003) 61-74.
12. P. Aguiar, C.S. Adjiman, and N.P. Brandon, J. Power Sources 138[1-2] (2004) 120-136.